Pérez-López, D.; Sánchez-Gomáriz, E.; Capmany Francoy, J. (2018). Programmable True Time Delay Lines Using Integrated Waveguide Meshes. Journal of Lightwave Technology. 36(19):4591-4601. https://doi.org/10.1109/JLT.2018.2831008

Programmable True-Time Delay Lines using integrated waveguide meshes

(Invited paper)

Daniel Pérez-López *Member, IEEE,* Erica Sánchez and José Capmany, *Fellow, IEEE, Fellow OSA*

***Abstract*— We analyze and explore the potential that waveguide-mesh-based architectures used in Programmable Photonic Integrated Circuits can be configured to enable true time optical delay lines, which can find applications in different Microwave Photonics functionalities, such as beamforming and optical filtering. We also propose and experimentally demonstrate an alternative standalone Tunable Basic Unit architecture where its internal coupling device is implemented by means of a Dual-Drive Tunable Directional Coupler (DD-TDC) that performs independent amplitude beamsplitting and phase shifting. Compared to the previous alternatives based on 3–dB Balanced Mach-Zehnder Interferometers (MZIs), the DD-TDC reduces by more than two times the insertion losses of TBUs enabling the potential realization of larger meshes with a three-fold enhanced step-time resolution. Bandwidth and robustness analysis are also considered.**

***Index Terms*—Microwave Photonics, Integrated optics.**

I. Introduction

Reconfigurable true time optical delay lines (TTODLs) are a key building block for a wide range of applications in optical processing when combined with optical couplers and phase shifters. Recent approaches based on cascading tunable couplers and discrete delay lines pursue compact and wideband discrete reconfigurable delays. These implementations are typically suitable for a single specification or application since the delays, even if they are tunable, are interconnected in a fixed configuration [1-6].

Programmable Multifunctional Photonics (PMP) [7-16] is a new paradigm that aims at designing common integrated optical hardware configurations, which by suitable programming can implement a variety of functionalities that, in turn, can be exploited as basic operations in many application fields. In contrast to application specific designs, where photonic integrated circuits (PICs) are designed to perform one single application, PMP provides more versatile cost-effective solutions and reduced the time-to market.

The most flexible approaches are based on waveguide mesh arrangements formed by replication of unitary cells (triangles, squares, hexagons, etc.) of 2x2 beamsplitters with additional phase shifting capabilities, that once configured, allow either only-forward [11-13], or both forward and backward signal propagation and routing through the mesh [9,10].

By suitable programming each 2x2 beamspliter or Tunable Basic Unit (TBU), both circuit topology and design parameters can be configured to implement tunable optical filters [9,14], beamforming networks, microwave photonic subsystems [16], universal linear optics operations [11-13, 15] and integrated quantum circuits [17]. In particular we are interested in this paper in exploring their suitability for implementing TTODLs.

In Section II, we address the basic definitions of waveguide meshes and identify the practical limitations related to their fixed basic delay and accumulated losses. In Section III, we illustrate different configuration examples of a waveguide mesh implementing programmable discrete tunable optical true time delay lines (DT-OTTDLs) for the particular example of an optical beamforming network. Section IV considers the implementation of programmable continuous tunable optical true time delay lines (CT-OTTDLs). There, we propose the use of the waveguide mesh to emulate the design based on balanced SCISSOR structures.

All the waveguide-mesh implementations proposed so far rely on TBUs implemented by means of balanced MZIs closed by 3-dB couplers. This TBU design offers a relatively wideband operation but the scalability of the circuit is limited due to the accumulated insertion losses (IL). Optimizing the TBU by miniaturizing the basic delay and the IL is essential to achieve high-frequency operation as well as reducing the total footprint of the circuit. In Section V, we propose an alternative TBU design based on a Tunable Directional Coupler with phase shifting capabilities. An analytical model is provided, simulated and experimentally validated for this structure. Our preliminary experimental results suggest that this design can lead to more compact designs with fewer insertion losses. Finally, Section VI summarizes and concludes the paper.

II. Waveguide-Mesh based Optical delay lines

In a similar way to the operating mode of electronic Field Programmable Gate Arrays, programmable PICs implementing multiport beamsplitters can be configured by discretizing conventional circuits into a previously fabricated waveguide

Manuscript received XXXXX, 2017; revised XXXX, 2015; accepted XXXX, 2017. Date of publication XXXXX, 2017; date of current version XXXX, 2017. "This work was supported in part by the European research Council under Grant ERC-ADG-2016-471715 UMWP-CHIP, the COST Action CA16220 EUWMP, the Spanish MINECO Projects TEC2014-60378-C2-1-R and the Gen. Valenciana PROMETEO Project 2017/103. Authors specially acknowledge VLC Photonics and the Centro Nacional de Microelectronica for the access to the Multi Project Wafer (MPW) run."

D. Pérez, E. Sanchez and J. Capmany are with the Photonics Research Labs, ITEAM Research Institute, Universitat Politècnica de València, Valencia, 46022 Spain (e-mail:dapelo2@iteam.upv.es, jcapmany@iteam.upv.es).

mesh arrangement of coupled waveguide pairs, known as TBUs, [9, 10]. By configuring each TBU, constructive, destructive or partial interference can be achieved at each complementary output port, leading to the routing of the signal and the definition of the circuit topology and design parameters. While sacrificing footprint, power consumption and optical gain, these circuits provide unprecedented versatility and flexibility, enabling applications that are not possible in standard application-specific PICs. Fig. 1 illustrates different combinations and waveguide mesh topologies that have been proposed in the literature for this purpose.

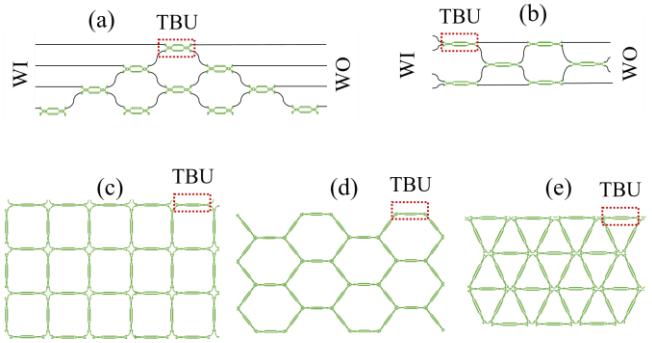

Fig. 1. Different waveguide mesh arrangements of beamsplitters: (a) Triangular Feedforward [11, 12], (b) Rectangular Feedforward [13], (c) Squared Feedforward/backward [9], (d) Hexagonal Feedforward/backward [10], and (d) Triangular Feedforward/backward [10]. WI/WO: Waveguide inputs/outputs.

The performance of the mesh arrangements in term of capabilities, time-step resolution, flexibility, versatility, power consumption and scalability depend both on the mesh topology and the TBU design. For time-dependent, high-resolution applications, the hexagonal waveguide mesh offers the best performance, [10, 18].

Fig. 2a illustrates a single hexagonal waveguide cell where the TBU are disposed in tri-lattices. As shown in Figure 2c, a generic TBU is defined by its access path lengths and a tunable coupler section that allows both independent power beam splitting and phase-shifting of light, [10]. The TBUs overall length is defined as its *Basic Unit Length* (*BUL*) and is related to the *Basic Unit Delay*, which will set an upper limit in terms of frequency operation as well as a limit in maximum time-step resolution of the overall mesh:

$$\tau_{TBU} = \frac{n_g \cdot BUL}{c}, \tag{1}$$

where c is the speed of light in vacuum, n_g is the waveguide group index.

In principle, an ideal lossless waveguide mesh is more powerful and versatile if the waveguide mesh is large enough to support the synthesis of complex PICs with a relatively large number of components and a finer waveguide discretization (short delays or short *BULs*). However, for real TBUs, their insertion losses (IL_{TBU}) will set a limit on the maximum number of TBU that can be traversed by the signal, limiting scalability of the meshes and the size of the programmed PICs.

We can define the figure IL_{TBU}/τ_{TBU} to measure the *loss per time unit* for a certain TBU. A signal propagating through a waveguide mesh, describing a path of $L=N$ *BUL*s operates as a delay line with $N\ IL_{TBU}$ accumulated loss and a delay defined by N τ_{TBU}. For example, in Fig. 2a, we could configure the TBUs to interconnect Points *P1* and *P2* either describing an upper path of 4 TBUs (L =4 BULs, 4 IL_{TBU}) or an alternative lower path of 6 TBUs, with a larger delay and greater loss. The signal flow for each splitting configuration is depicted in Fig. 2b.

If we require a finer step resolution and desire to synthetize the same previous length L, but using a miniaturized waveguide mesh with a shorter *BUL*, we would need a greater number N of TBUs to program the path (or delay), as obviously:

$$N \propto \frac{L}{BUL}. \tag{2}$$

In the realistic case of considering non-zero TBUs losses for a desired length L (or *delay)*, the accumulated losses are greater for miniaturized waveguide meshes.

A common feature of waveguide meshes demonstrated so far is the use of balanced MZIs to implement the TBUs, either using multimode interference or directional couplers for the two required 3-dB couplers, as illustrated in Fig. 2.d1. In this device, the splitting ratio is defined by the differential phase shift applied to each arm of the MZI. An additional common phase shift to each arm enable an independent phase setting of the overall structure, [9, 10]. The two required 3-dB couplers limit its footprint and dominate the total accumulated insertion losses for a defined path.

$$IL_{TBU} \approx 2IL_{Coupler} + \alpha\left(dB/cm\right)\cdot BUL\left(cm\right), \tag{3}$$

where α is the propagation loss. With this approach, a programmed waveguide length containing N TBUs will always have $2N\ IL_{coupler}$ additional losses compared to that of a standard waveguide in the same integration platform, with accumulated losses referred in the right-side of the summation of (3).

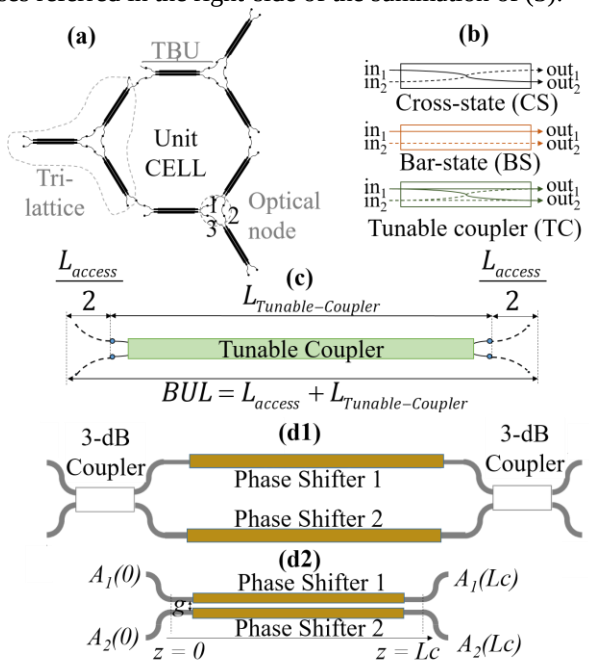

Fig. 2. (a) Labeled Hexagonal Unit Cell. (b) Signal flow for the different TBU configuration (c) Schematic of a general tunable coupler acting as the basic building block of the mesh: Tunable Basic Unit (TBU). The Basic Unit Length is illustrated as the sum of the tunable coupler length and the arc length of the access waveguides. A particular case of a tunable coupler implemented by (d1) a MZI and (d2) an integrated dual-drive tunable directional coupler.

Fig. 2.d2 illustrates an alternative TBU design based on a Dual-Drive tunable directional coupler, where both the splitting ratio and the total phase response can be tuned independently. In this case, the insertion losses are reduced considerably, since only one coupler is employed. This device is described and thoroughly analyzed in Section V. In the next sections, we will consider a generic-TBU for functional operation.

III. Programmable Optical Delays

A. *Optical Beamforming Configurations:*

Optical delay lines are the key element in a wide variety of functionalities, for example, in beamforming networks for phased array antennas. These devices modify the radiation characteristics of an array of equal radiating elements simply by changing their field excitations. The beam is then steered by adjusting the phase relationship between the different feeding paths. The angle of transmission or reception θ is given by [19]:

$$\theta = \arcsin\left(\frac{\lambda \cdot \Delta\phi}{2 \cdot \pi \cdot d}\right), \qquad (4)$$

where d is the distance between array radiating elements, λ the optical wavelength and $\Delta\phi$ is the differential phase shift introduced between the different array elements, as illustrated in Fig. 3. There are two alternatives to perform the phase shift. The first one is by directly applying the differential phase by an integrated phase shifter. In this case, the pointing angle varies with the input RF frequency causing beam squint. The second approach is to use tunable true time delay lines, where the pointing angle θ remains independent of f_{RF} offering a squint-free approach suitable for wideband operation, [19, 20].

The TTODL operation can be programmed in waveguide meshes by configuring some of the TBUs as tunable couplers and some as optical crossbar switches, creating adjacent light-paths with an incremental length value ΔL (expressed in discrete values of BULs). This incremental length defines, in turn, the tilt angle of the antennas placed at the outputs, together with the distance between the radiating elements.

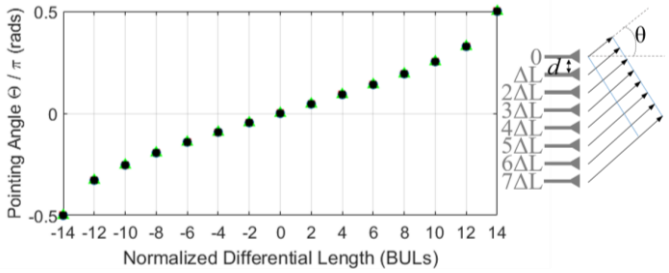

Fig. 3. Tilt angle variation in a beamforming network based on discrete delay line implementation for broadband operation versus normalized differential length. For this example, the distance between radiating elements d = ng 14 BUL, to split the tilt angle range in 15 discrete steps of 2 BULs. (Right) Output ports and wave-front angle definitions.

The upper part of Fig.4 illustrates the programmed configuration of two discrete delay lines enabled by a hexagonal mesh featuring paths of 5 and 11 BULs, respectively. The lower part of the figure displays the measured results obtained by enabling different paths in a recently reported SOI chip where TBUs were implemented using 3-dB MZI-based TBUs, [14]. The basic delay provided by a BUL is 13.5 psec and the figure shows the successful implementation of delays ranging from 3 to 12 BULs. Note that the amplitudes of the different delayed pulse replicas are different, which is due to the different losses experienced by the signal as it propagates through different paths. In particular, the logarithmic power response vs length (time) was measured to be approximately linear with a decaying rate of 0.59 dB per BUL (per 13.5 ps). Errors in the fitting are mainly related to variations in grating coupler losses (±0.5 dB) and to a lesser extent in TBU losses (<0.1 dB), [14]. Note that different input/output ports combinations where employed. Nevertheless, these amplitudes can be equalized (though not sown in the figure) using the ability of TBUs to independently tune their coupling constant values.

For a fixed d, the pointing angle is limited to discrete values that can be varied modifying the differential lengths between each feeding network segment (ΔL). Fig. 3 shows the tilt angle for a normalized TBU, where the distance between radiating elements is chosen to fix $\theta = \pi/2$ for a *normalized differential length* of up to ΔL = 14 BULs. A step of 2 ΔL is employed. In the case of fixed d, larger BULs produce less angle resolution. Note that "negative" waveguide lengths refer to the case where the lower antennas have a shorter feeding path. In this example, the angle range is divided in 15 different positions.

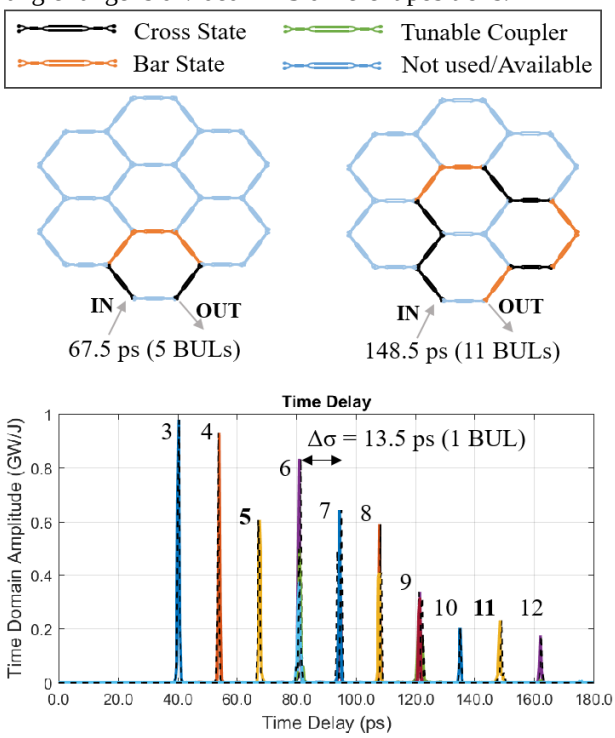

Fig. 4. Discrete optical delay lines implemented in a 7-cell layout: (up) settings for two different time delays describing 5 and 11 BULs. (Bottom) Measured delays up to 12 BULs.

If a continuous tuning is necessary, continuously tunable delays need to be added to provide a finer angle tuning, [4]. One possible option for this fine tuning is described in the next section. If a certain application requires the feeding of a higher number of antennas to enable, for example, 2D tunability, additional mesh-based PICs can be employed.

Fig. 5 illustrates, as an example, the implementation of a 1x8 beamforming network based on a hexagonal waveguide mesh

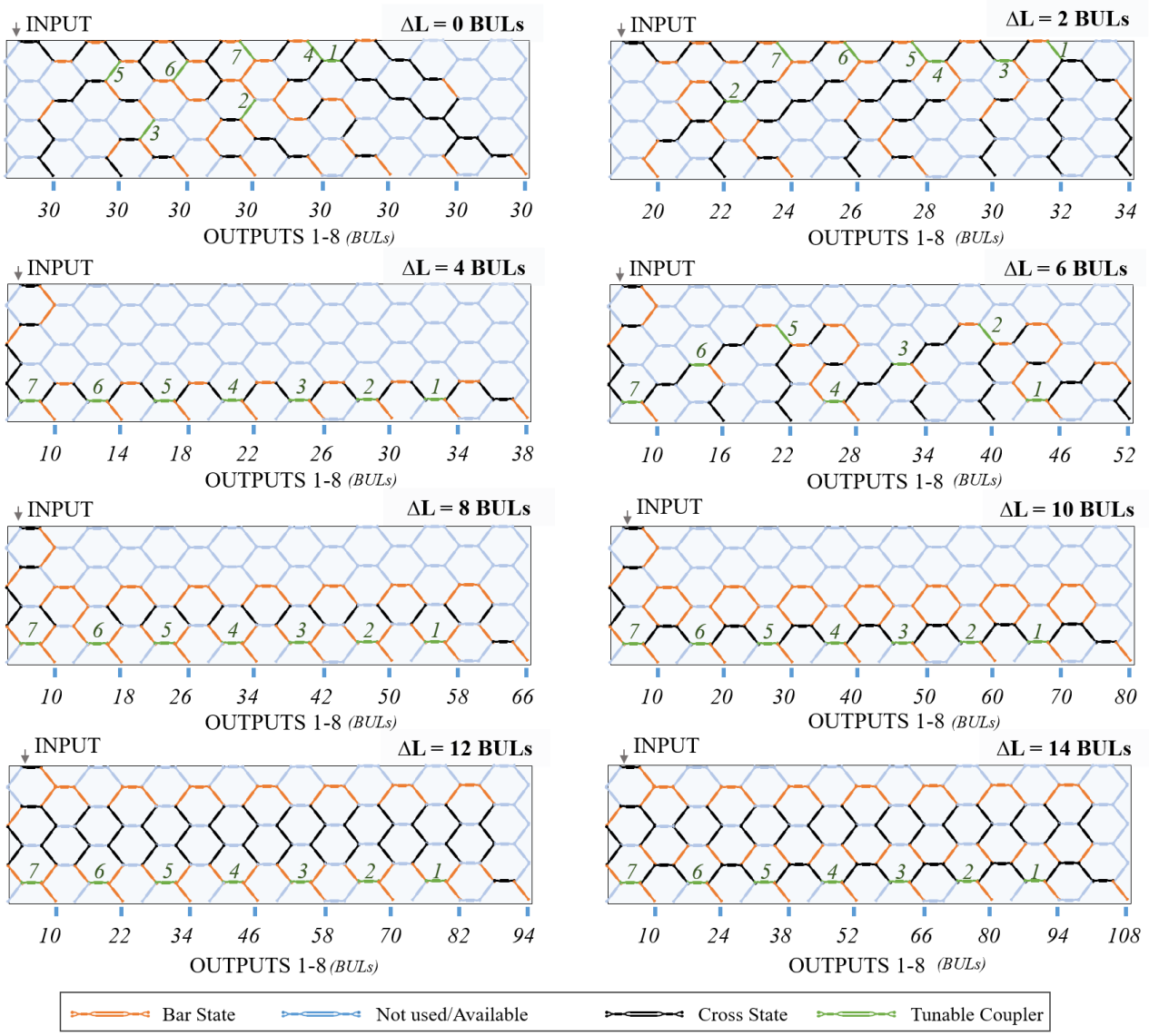

Fig. 5. 1X8 Beamformer based on discrete optical delay lines: Configuration examples for 0-, 2-, 4-, 6-, 8-, 10-, 12-, and 14-BUL path difference. Each path length is labeled at each output. The color-coded used for each TBU configuration is: Cross State (black), Bar State (Orange), Tunable Coupler (Green). For each Tunable Coupler mode, a number is given for its reference to the Appendix A and to (5).

in a PIC layout. By suitable configuring each TBUs using the defined color-code for crossbar and tunable coupling operation we illustrate the beamformer operation for different differential delays. In particular, for path length differences of 0, 2, 4, 6, 8, 10, 12, and 14 BULs. For each delay configuration, we have specified at each output port, the corresponding number of TBU that define the delay. As outlined in the previous section, larger delays suffer from greater losses. These can be compensated by tailoring the coupling constants of the TBUs configured as a tunable couplers. Note that there are seven TBUs in Tunable Coupler mode for each configuration, labeled and shown in green color.

By means of the following, each of these tunable couplers will compensate for the unbalanced subsequent path losses according to:

$$K_n = \frac{1}{10^{\frac{L_{n,bar} - L_{n,cross}}{10}} + 1}. \qquad (5)$$

Here n=7,6…1, denotes the Tunable Coupler number and $L_{n,bar}$ and $L_{n,cross}$ represent the accumulated losses from the output of each coupler to their corresponding beamformer output port. We can differentiate two cases for the definition of the *accumulated loss*: First, if the path from the output of the tunable coupler n is only configured by TBUs in switching states (either cross or bar), then the accumulated loss in this port is:

$$L_{n,bar/cross} = N \cdot IL_{TBU}, \qquad (6)$$

where N is the number of TBUs from the tunable coupler to the corresponding port. As an example, the coupler number two in Fig. 5 (for the case of ΔL =8), has accumulated losses in the lower port (*cross)* given by $L_{n,cross}=IL_{TBU}$, since there is only one TBU in bar switching state in the interconnection path. Secondly, if the path from the output of Tunable Coupler n and the beamformer port includes at least one Tunable Coupler TBU, then the nearest one is labeled as coupler q and:

$$L_{n,bar/cross} = 10\log_{10} K_q + (r+1)IL_{TBU} + L_{q,cross}, \qquad (7)$$

where r is the number of TBUs between coupler n and coupler q. An example of this case can be observed in Fig. 5 (for the case $\Delta L = 8$), where the path connecting the upper (*bar)* port of coupler number two to beamformer outputs 7 or 8 includes one of the TBUs configured as a Tunable Coupler.

Note that if it is possible to access the mesh both from the right and left (Fig. 5), then the applied configurations can be mirrored in the vertical axis to allow a complete [-π, π] tilt range.

To estimate the performance of this mesh we will assume four TBU cases that are potentially achievable considering the state of the art and summarized in Table I.

TABLE I
CASES OF STUDY FOR DIFFERENT ARCHITECTURES AND PLATFORMS

Case	Material (ng)	Architecture	BUL(μm)	IL(dB)	Δτ (ps)
A	SOI, (4.18)	MZI	300	0.20	4.18
B	SOI, (4.18)	TDC	100	0.05	1.39
C	SiN, (1.93)	MZI	1000	0.20	6.43
D	SiN, (1.93)	TDC	700	0.05	4.50

Here we have assumed propagation losses below 2 dB/cm and 1 dB/cm in SOI and SiN, respectively, and ultra-low loss 3-dB couplers, [21-24]. Note that in silicon nitride platforms, the phase shifters can be designed exploiting the thermo-optic effect. Thermal tuners in SiN require device length larger than 600 μm to ensure a 2π-phase shift [25], while this number is below 100 μm in SOI platforms [26]. Optimizing these structures or even migrating to alternatives tuning effects like opto-mechanics help to reduce the length and the crosstalk associated to the tuning [27-29], if needed. Fig. 6 illustrates the accumulated losses for each port after compensation carried by (5) for each case. We will find a total accumulated loss associated to propagation and splitting at each port corresponding to 25 and 12.27 dB for worst cases A&C, and B&D, respectively. Note that the B/D cases are dominated by the splitting losses corresponding to 9.03 dB that would be equally present in a standard application-specific PIC design. The resulting coupling values for each configuration can be found in Appendix A.

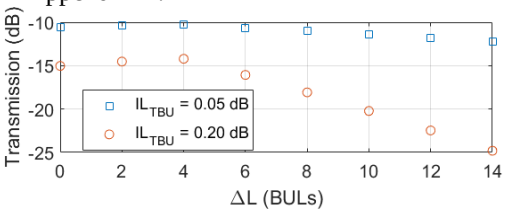

Fig. 6. Transmission losses for two different TBU losses at every output port versus path length difference for the designs in Fig. 5.

Optical Beamforming networks based on providing a differential phase shift to each output can be as well programmed in the hexagonal-mesh core, either by using a tree-scheme with a phase shifter at each output or by programing a linear interferometer for the beamsplitting section. This case is suitable for low bandwidth applications since the output signal frequency and the tilt angle are not independent.

The non-desired side effects related to the use of non-ideal components result in additional insertion losses and additional optical crosstalk due to the drift in the configured coupling value and to fabrication or design errors. The optical crosstalk produces signal leaking through the overall mesh that causes reflections inside the circuits, creating ripples in the spectral response. These are the main drawbacks when compared to application specific Photonic Integrated Circuits and were briefly analyzed in [16, 18]. An extensive modeling and analysis method is under current final development, and will be reported in the near future. This method allows the evaluation of the impact of crosstalk and non-ideal circuit parameter setting on the performance of complex waveguide mesh. Due to the extension of developed method and space constrains of the paper, we here highlight two main results obtained after its application to the 1x8 beamformer of Fig. 5: first, the unused TBUs can be configured to extract the leaked signal to drain optical ports to radically improve the system performance. Secondly, TBUs with optical crosstalk less than 20 dB are highly desirable to maintain good circuit performance.

IV. CONTINUOUSLY-TUNABLE DELAY LINES

Continuously tunable optical true time delay lines (CT-OTTDLs) prone to be integrated on a chip can be implemented using the strong resonances provided by several ORRs. In particular both CROW and SCISSOR configurations can be used but the latter is more robust against variations in the structure parameters due to fabrication errors. The basic theoretical ground for the implementation of SCISSOR based CTTDLs can be found in [4]. A strong limitation of strong resonances is that they are very dispersive, and thus characterized by a strong group delay dispersion (GDD), which limits their operational bandwidth. A solution to overcome this limitation is to employ a balanced SCISSOR configuration, where one half of rings have their resonant frequencies shifted up by a small amount $\Delta\omega$ relative to the central signal frequency ω_0, while the resonance frequencies of the other half are shifted down by the same amount, i.e., $-\Delta\omega$. Ring cavities are then grouped in N pairs as shown in Fig. 7(a), where the up- and the down-shifted rings are located on opposite sides of the same bus as this is the simplest way to implement the required resonance shift using either thermal or carrier-induced phase shifts in the cavities avoiding crosstalk. Fig. 7(b) shows how the waveguide mesh can naturally emulate this structure with the adequate TBU programming. This implementation brings several advantages. First, the required phase shifters do no need to be distributed along the entire ring cavity but can be implemented by a single TBU unit allocated in its perimeter. Then the location of this TBU can be chosen so it is far enough from the others so thermal or electric crosstalk is minimized. This is also shown in Fig. 7(b). In second place, TBUs acting as tunable couplers can be programmed to provide variable coupling ratios and therefore more flexible operation by giving access to various regimes that allow different tunable delay ranges and operation bandwidths as shown in [6].

A third advantage is that by suitable TBU programming the cavity lengths can be changed and thus the value of the basic ring cavity delay. Furthermore, if desired, several balanced

units can be switched off just by setting their coupling constants to unity (bar state). This again provides a further degree of flexibility by allowing the access to an upper limit in the available delay or by setting incremental delays using the same CTTDL architecture.

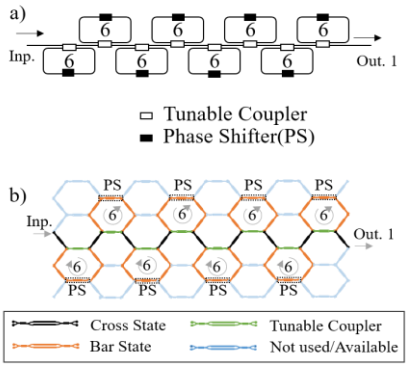

Fig. 7. (a) Continuously tunable true time delay unit based on a balanced SCISSOR architecture. (b) Implementation using the hexagonal waveguide mesh.

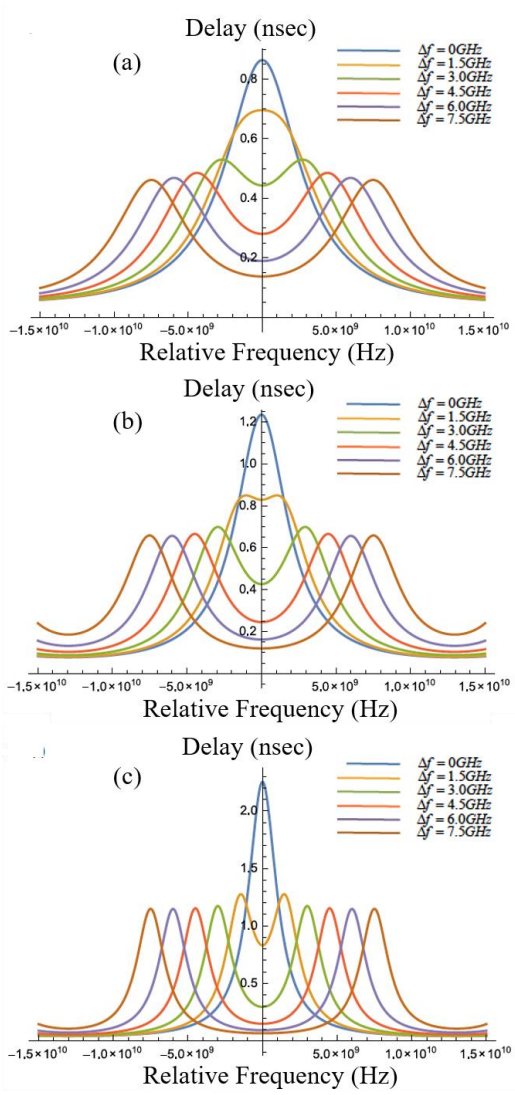

Fig. 8. Calculation of the continuous group delay vs frequency dependence for a 8 varied Balanced SCISSOR CTTDL structure versus the frequency detuning Δf for different cases (a) K=0.8 and $\Delta\tau$ =4.5 psec, (b) K=0.8 and $\Delta\tau$ =6.4 psec, (c) K=0.65 and $\Delta\tau$ =6.4 psec.

As an example, Fig. 8 shows the results of a numerical analysis of a balanced 8-unit SCISSOR CTTDL implemented by a hexagonal waveguide mesh featuring TBU delay parameters provided in Table I. Note that the total cavity delay is given by τ=6 $\Delta\tau$.

The upper part of Fig. 8 represents the continuous group delay tuning for the case of a Si_3N_4 hexagonal waveguide mesh where the TBUs are implemented by means of directional couplers with K=0.8 and $\Delta\tau$ =4.5 psec (τ= 27 psec), while the lower case represents the case where the TBUs are implemented by means of Mach-Zehnder interferometers where K=0.8 and $\Delta\tau$ =6.4 psec (τ=38.4 psec). This last case is very similar to that reported in [6] using Si_3N_4 ring cavities which feature a value of =40 psec. In fact, Fig. 8(c) represents the same case of 9(b) when the coupling constant is changed from k=0.8 to k=0.65. As predicted in [6] (figure 12) the group delay range in this case is increased at the expense of a reduction in the operational bandwidth.

V. Tunable Directional Coupler Waveguide Meshes For Compact OTTDLs

In the previous sections, we have illustrated why a waveguide mesh circuit becomes impractical when it is made of TBUs with high or moderate insertion losses. Due to the considerable number of TBUs that would need to be traversed by the signal in a circuit with certain degree of interconnection complexity, a minimum improvement in the TBU design leading to a reduction in their insertion losses will have a remarkable impact on the overall mesh design and performance. To achieve this, we analyze here the possibility of implementing the TBUs using a tunable directional coupler with two phase shifters instead of a 3-dB MZI.

A. Concept

The directional coupler is one of the most employed building blocks present at any PIC. It is usually designed to operate as a beamsplitter featuring a desired fixed optical power splitting ratio K at a certain wavelength. The signal of one waveguide is totally transferred to a parallel waveguide at each periodic length Lc with a coupling constant κ that depends on the wavelength, the waveguide geometry and the refractive indexes of the materials. This dependency aggravates the DC tolerance to fabrication errors that change the designed wavelength of operation, bandwidth and uniformity.

Standalone Tunable Directional Couplers (TDC) have been demonstrated in polymer materials [30-33], photonic crystals [34] and in Silicon on Insulator [35], providing a reconfigurable splitting ratio by enabling a propagation constant difference in the pair of waveguides by means of a thermal-tuner placed on top of one of the parallel waveguides or by applying electro-optic effect to introduce a propagation constant difference between the waveguides.

In order to increase the capabilities of TDCs, the integration of a second phase shifter in the other waveguide provides both an independent beamsplitting and additional phase shifting capabilities by inducing a differential and common phase shift, respectively, on each waveguide, enabling their used as a TBU

in waveguide mesh PICs. A cross-section of the thermally-tuned Dual-Drive TDC view is illustrated in Fig. 9.

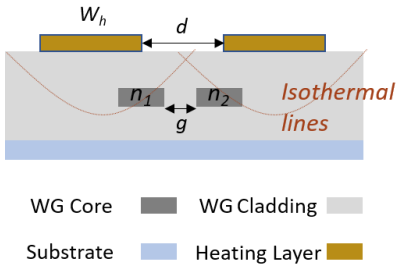

Fig. 9. DD-TDC cross-section. *d*: distance between heating layers, *g*: gap between waveguides.

B. Analytical Model

By applying coupling mode theory [36], the optical field at the output of a TDC results in:

$$A_1(z) = e^{j\left(\frac{\beta_1+\beta_2}{2}\right)z}\left\{\begin{array}{l}\cos\left[\frac{z}{2}\sqrt{\Delta^2+4|\kappa|^2}\right] \\ -j\frac{\Delta}{\sqrt{\Delta^2+4|\kappa|^2}}\sin\left[\frac{z}{2}\sqrt{\Delta^2+4|\kappa|^2}\right]\end{array}\right\} \quad (8)$$

$$A_2(z) = e^{j\left(\frac{\beta_1+\beta_2}{2}\right)z}\frac{2j\kappa}{\sqrt{\Delta^2+4|\kappa|^2}}\sin\left[\frac{z}{2}\sqrt{\Delta^2+4|\kappa|^2}\right],$$

where β_1 and β_2 are the propagation coefficients of the modes in the two guides, and κ is the coupling coefficient between modes, z,is the variable that defines the coupling length and Δ is the propagation coefficients difference β_1- β_2. The squared-modulus and phases responses are:

$$\begin{aligned}|A_1(z)|^2 &= \left(\begin{array}{l}\cos^2\left[\frac{z}{2}\sqrt{\Delta^2+4|\kappa|^2}\right]+ \\ \frac{\Delta^2}{\Delta^2+4|\kappa|^2}\sin^2\left[\frac{z}{2}\sqrt{\Delta^2+4|\kappa|^2}\right]\end{array}\right) = \\ &= \alpha_{TBU}\sqrt{1-K^2} \\ |A_2(z)|^2 &= \frac{4|\kappa|^2}{\Delta^2+4|\kappa|^2}\sin^2\left[\frac{z}{2}\sqrt{\Delta^2+4|\kappa|^2}\right] = \\ &= \alpha_{TBU}K,\end{aligned} \quad (9)$$

$$\begin{aligned}\mathrm{Arg}\left[A_1(z)\right] &= \left(\begin{array}{l}\left(\frac{\beta_1+\beta_2}{2}\right)z \\ -\tan^{-1}\left\{\frac{\Delta\tan\left[\frac{z}{2}\sqrt{\Delta^2+4|\kappa|^2}\right]}{\sqrt{\Delta^2+4|\kappa|^2}}\right\}\end{array}\right) \\ \mathrm{Arg}\left[A_2(z)\right] &= \left(\frac{\beta_1+\beta_2}{2}\right)z+\frac{\pi}{2},\end{aligned} \quad (10)$$

Propagation coefficients include a real part and an imaginary part for the losses. In addition, we can separate a static contribution, that accounts for the passive behavior of the waveguides (referenced as subindex *p*) and an active contribution from the phase shifters to each waveguide (β_a) given by the change in the effective index Δn_{eff}.

$$\begin{aligned}\beta_1 &= (\beta_{1p}+\beta_{1a})+j(\alpha_{1p}+\alpha_{1a}), \\ \beta_2 &= (\beta_{2p}+\beta_{2a})+j(\alpha_{2p}+\alpha_{2a}).\end{aligned} \quad (11)$$

For this analysis we will employ thermal-tuners as our active element. Since this mechanism can be designed to avoid additional tuning losses we can compute Δ as:

$$\begin{aligned}\Delta &= (\beta_{1p}-\beta_{2p})+(\beta_{1a}-\beta_{2a})+j(\alpha_{1p}-\alpha_{2p}) \\ &= \Delta_p+\Delta_a+j(\alpha_{1p}-\alpha_{2p}),\end{aligned} \quad (12)$$

Considering (9-12), we can see that modifying the propagation constant β_a, we introduce a phase shift in one of the waveguides that changes the coupling constant of the directional coupler *K*. This effect has been experimentally demonstrated for switching operations in [5, 6, 7].

Looking again into the previous equations, it can be shown that a common increment in both waveguides, i.e. $\beta_{1a}=\beta_{2a}$, leads to a fixed splitting ratio operation while the phase response is tuned accordingly.

The design length depends on the desired power splitting value *K*. For passive cross-DCs, where both waveguides are equal, i.e. $\Delta\beta_{1p}=\Delta\beta_{2p}$, the length should be equal to:

$$L_{co} = \frac{\pi}{2|\kappa|}, \quad (13)$$

If the parallel waveguides are different, i.e. $\Delta\beta_{1p} \neq \Delta\beta_{2p}$, then a correction factor should be imposed to the coupling length, resulting in:

$$L_{co,2} = \frac{L_{co}}{\sqrt{\left(\frac{\Delta\beta L_{co}}{\pi}\right)^2+1}}, \quad (14)$$

For 3-dB couplers, the coupler length is half of the total coupling length. In the access waveguides, the signal is coupled. This effect must be considered by decreasing L_{co}. In the following analysis we will neglect this contribution, i.e L_{co} will refer to the effective length of the coupler rather than the physical length.

C. Passive Analysis

In order to analyze the performance of the proposed TDC and to illustrate the previous concepts, we have simulated with a mode-solver the crossection structure for different geometries of width, height, and gap variations in a SiN platform [37]. Next, we applied the data to the model and obtained the spectrum characteristics before its processing.

From the simulated values, the resulting total coupling length for each gap for a wavelength of 1.55 μm are shown in Table II:

TABLE II
SIMULATED DC COUPLING LENGTH VALUES FOR DIFFERENT GAPS AT A WAVELENGTH OF 1.55 μm.

Gap (μm)	0.6	0.8	1.0	1.2	1.4	1.6
(w=1μm) L_{co} (μm)	58.2	101.7	180.6	311.2	543.7	945.4
(w=1.2 μm) L_{co} (μm)	90.6	163.6	301.2	565.0	1002.4	1852.3

We can observe that the closer are the waveguides, the shorter will be the DC, as one would have expected, since the interaction between waveguides is stronger.

For each of the previous configurations, Fig.10 illustrates the bandwidth variations for passive cross-DC and 3-dB DCs. We obtained bandwidth values ranging from 45-20. Once we have chosen some certain design specifications, fabrication errors might differ from the material properties assumed in the design stage as well as geometrical properties: waveguide width, height, and gap variations. For example, we have simulated 600±20 nm gap variations that result in a center wavelength variation of 0.86 (wavelength (nm)/gap(nm)) and 1600±20 nm gap variations that result in 0.53 (wavelength (nm)/gap(nm)). Although it seems that separated waveguides are more robust to gap variations, the bandwidth is significantly reduced.

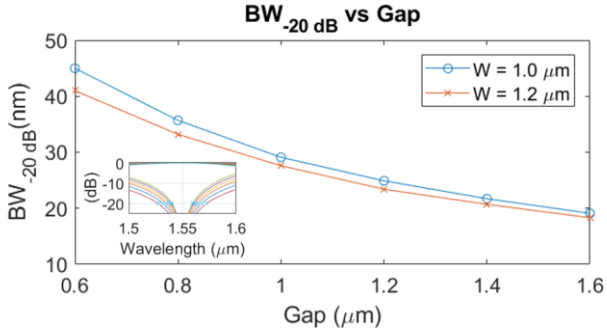

Fig. 10. Bandwidth versus gap for different directional couplers: Cross Directional coupler for the lengths specified in Table 1. The inset illustrates the spectral response for the optical power transmission of both output ports.

Several techniques have been proposed, mainly in SOI platforms to increase the fabrication tolerances as well as the bandwidth of DCs [24, 38, 39] that could be extended to TDC in SOI and SiN platforms.

D. Thermo-Optic Tuning Analysis

The phase shift can be impressed into the lightwave by exploiting different tuning effects. The most common is the thermo-optic effect since if it is properly designed, the tuning mechanism do not incorporate additional losses to the structure. It consists on placing a thin metal layer over the waveguide. By applying Joule effect, the electrical power is transformed into heat that increase the temperature at the waveguide and produces a change in the effective index.

The main drawback, is that since both waveguides are too close, undesired heat flow will heat the second waveguide as well. This effect is characterized by a thermal crosstalk coefficient ($CT_{Thermal}$), where:

$$\beta_{1a} = \frac{2\pi}{\lambda}\Delta n_{eff} = \frac{2\pi}{\lambda}\frac{\partial n_{eff}}{\partial T}\Delta T_{c1},$$
$$\beta_{2a} = \frac{2\pi}{\lambda}\frac{\partial n_{eff}}{\partial T} CT_{thermal}\Delta T_{c1}. \quad (15)$$
$$\Delta_a = \frac{2\pi}{\lambda}\frac{\partial n_{eff}}{\partial T}\Delta T_{c1}\left(1 - CT_{thermal}\right)$$

We performed thermal simulations to obtain the optimum distance d to maximize the temperature gradient between waveguide cores for different waveguide gaps and the temperature difference variation for different heater temperatures. These results are similar to the ones obtained in [33, 35] for different material platforms. As shown in Fig. 11, in these cases the function maximizes for distances between 1.71 and 1.94 μm. This temperature gradient difference also depends on the heater width, which in this case is fixed to 4 μm. The heater width is mainly limited by the foundry specifications. Moreover, a constrain related to the minimum distance between metal layers is imposed by the fabrication process to ensure that the metal opening is properly achieved.

Considering the effect of a differential phase shift Δ, the splitting ratio can be set as demonstrated in Fig. 12. Here, we can see a TDC in passive cross state characterized by a gap of 1580 nm and a length of 894.89 μm. For a CT of 0.6, the bar state is achieved for a $\Delta n_{eff,1}$ of $3.8\cdot10^{-3}$ in the waveguide 1, whereas if a CT of 0.75 applies, the required value is $6\cdot10^{-3}$.

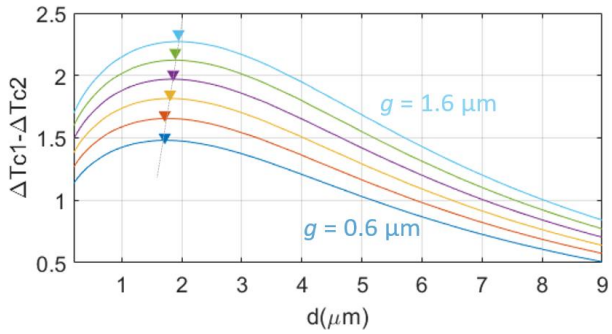

Fig. 11. Temperature difference between both waveguide cores when the $Heater_1$ increases its temperature 10ºC versus distance between heaters. Traces for different waveguide gaps from 0. 6 to 1.6 μm are displayed with their maximum. They correspond to CT between 0.6 and 0.75.

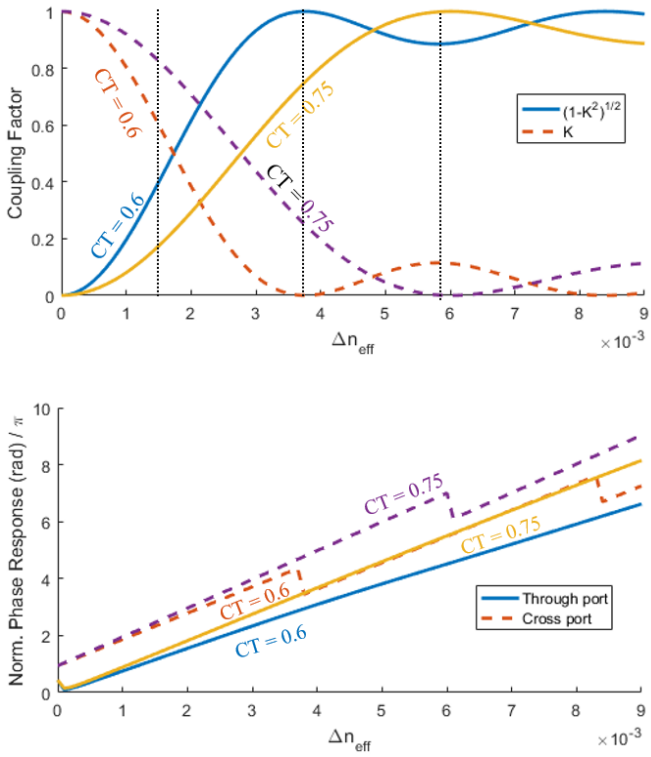

Fig. 12. Tuning response: Coupling factor (top), and phase tuning (bottom) vs effective index change in waveguide 1 for different CT values for Tunable Directional Coupler in passive cross-state.

Note that the overall phase response will change with $\Delta n_{eff,1}$ if only one of the phase shifters is employed.

In Fig. 13 we illustrate that once a fixed splitting ratio is configured, for example, 40:60 ($\Delta n_{eff,1} = 1.5 \cdot 10^{-3}$) for a CT = 0.6, the overall phase can be tuned if a common $\Delta n_{eff,common}$ is added to both waveguides. Note that the slope is greater since in this case, the thermal crosstalk contributes to both waveguides equally. This common phase shift is essential for implementing tunable optical filters, waveguide mesh arrangements and for correcting phase errors during fabrication.

It is worth mentioning that the minimum bandwidth during its operation is given by the passive cross-state. As long as the splitting ratio is tuned, the bandwidth tends to a single-isolated waveguide response. For this particular example, the bandwidth grows from a 2%-Bandwidth of 28.8 nm to more than 100 nm.

Moreover, (9) predicts that the bar response is achieved periodically in the tuning process, as verified in Fig. 13. This is not the case for the cross state, that can only be achieved if it is properly designed for an initial passive cross-state.

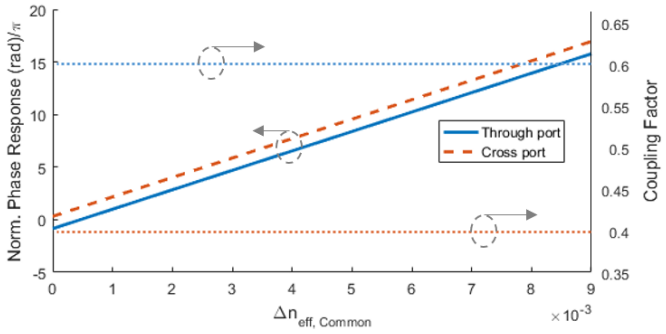

Fig. 13. Tuning Phase response: Fixed coupling factor 40:60 and phase tuning (bottom) vs common effective index change for a CT = 0.6 in a Tunable Directional Coupler in passive cross-state.

E. Experimental demonstration

For the experimental validation of the previous model, we have designed and fabricated under a Multi Project Wafer (MPW) run offered by the Centro Nacional de Microelectronica (CNM) and VLC Photonics [25, 37] a standalone Dual-Drive Tunable Directional Coupler in a silicon nitride platform, illustrated in Fig. 14. For the measurements we employed a tunable laser sweeping from 1520 to 1620 nm, followed by a polarization controller before accessing the chip by means of lensed fibers. The data was acquired by an optical spectrum analyzer for each programmed electrical power value.

In this case, a single-mode waveguide of 1 µm width and 300 nm height was employed to propagate a TE field. As illustrated in Fig. 9, the gap between the waveguides (g) was set to 1.5 µm, leading to a theoretical total coupling length of 717 µm. However, we decided to increase the final coupler length L to 1235 µm to increase the safety of the thermal tuners and to check the analytical model rather than to find a perfect passive-cross state, and before proceeding to an optimization round. For the metal layer, a distance between heaters (d) of 2 µm was considered. The optical crosstalk was kept between 15-21 dB for the cross and bar operations while obtaining a bandwidth > 5 nm for a ±2% uniformity. The total excess loss was negligible and estimated to be under 0.1 dB. Fig. 14b illustrates the change of K versus applied electrical current at four different wavelengths. The model was validated and predicts fabrication errors in the range of 15 nm width and 70 nm gap variation.

For this particular proof of concept device, the power consumption needed for the coupling factor reconfigurability from 1 to 0 is greater than in a MZI approach if a thermal tuning mechanism is employed (i.e we measured a power consumption of 270 mW for the MZI approach and estimate a 460 mW for the TDC approach in the same integration platform). The reason behind this is the proximity of the two waveguides and the resulting un-optimized thermal crosstalk that impacts more seriously the common rather than the differential phase shift. However, if the structure is optimized accordingly by changing d and g, the electrical power consumption can be considerably reduced [24, 27]. With the state-of-the-art, TDCs with phase shifting capabilities of less than 700 µm and 100 µm in silicon nitride and silicon on insulator platforms could be achieved, respectively, which represent more than a three-fold length decrement with respect to the MZI-based TBU approaches. In addition, alternative tuning mechanisms like electro-mechanical effect seems a promising option to achieve low-power, low-loss and shorter TDCs, [28, 29].

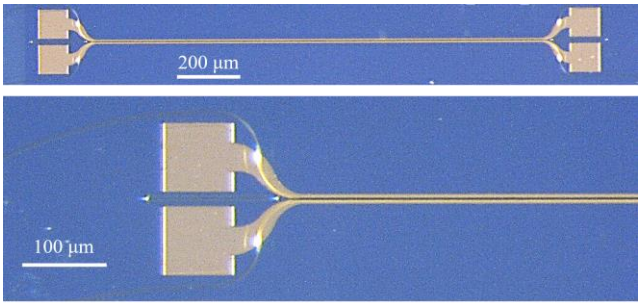

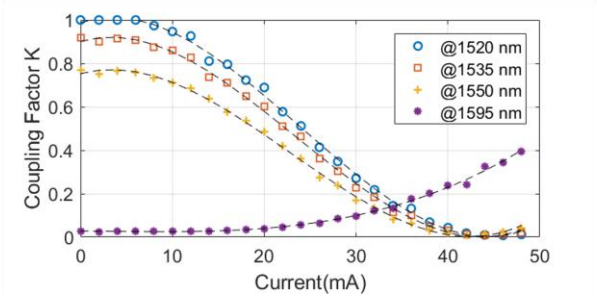

Fig. 14. TDC picture and experimental results of the tunable directional coupler coupling factor versus current applied to one of the phase shifters for different wavelengths. A cubic fitting is added for each trace (dashed).

VI. Summary, Conclusions and Future Challenges

We have proposed the use of hexagonal integrated waveguide mesh configurations for the implementation of compact discrete and continuous programmable OTTDLs. These structures are built upon tunable basic units (TBUs) that provide a tunable connection between two waveguides.

To program complex and large OTTDLs systems, such as those required in optical beamforming applications, even moderate TBU losses (0.25 dB/TBU) seriously degrade the overall circuit performance. To overcome this limitation, we have proposed to replace the current TBU design based on 3-

dB MZI devices by Tunable Directional Couplers incorporating two independent phase shifters (one per waveguide). With this new TBU design the losses in the waveguide mesh circuit are comparable to those of similar OTTDLs designed using Application Specific Photonic Integrated Circuits (ASPICs). When compared to the balanced 3-dB MZI TBU approach, we find at three-fold enhanced step-time resolution as well. Preliminary experimental proof of concept results in a Si_3N_4 TDC design show promising results, which can be further improved in terms of TBU length and operation power if alternative tuning mechanisms are successfully developed.

VII. Appendix A

Table. A1. Coupling Values for each Path difference length. IL = 0.20 dB.

	ΔL (BULs)							
K	0	2	4	6	8	10	12	14
K1	0.500	0.523	0.454	0.431	0.409	0.387	0.365	0.344
K2	0.500	0.470	0.274	0.247	0.221	0.196	0.174	0.153
K3	0.500	0.697	0.186	0.158	0.132	0.110	0.091	0.074
K4	0.667	0.783	0.134	0.107	0.084	0.065	0.050	0.038
K5	0.333	0.835	0.100	0.075	0.055	0.039	0.028	0.019
K6	0.600	0.869	0.077	0.054	0.037	0.024	0.016	0.010
K7	0.375	0.814	0.060	0.039	0.025	0.015	0.009	0.005

Table. A2. Coupling Values for each Path difference length. IL = 0.05 dB.

	ΔL (BULs)							
K	0	2	4	6	8	10	12	14
K1	0.500	0.506	0.488	0.483	0.477	0.471	0.466	0.460
K2	0.500	0.494	0.318	0.311	0.303	0.296	0.288	0.281
K3	0.500	0.674	0.233	0.225	0.217	0.209	0.201	0.193
K4	0.667	0.759	0.182	0.173	0.165	0.157	0.149	0.141
K5	0.333	0.809	0.148	0.139	0.131	0.123	0.115	0.107
K6	0.600	0.843	0.124	0.115	0.107	0.099	0.091	0.084
K7	0.375	0.767	0.106	0.097	0.089	0.081	0.073	0.066

References

[1] X.Wang *et al*., "Continuously tunable ultra-thin silicon waveguide optical delay line," *Optica*, vol. 4, num. 5, pp. 507-515, 2017.

[2] R.Moreira, *et al., "*Programmable eye-opener lattice filter for multi-channel dispersion compensation using an integrated compact low-loss silicon nitride platform," *Optics express*, vol. 24, num. 15, pp. 16732-16742, 2016.

[3] K. Jinguji y M. Kawachi, "Synthesis of coherent two-port lattice-form optical delay-line circuit," *Journal of Lightwave Technology*, vol. 13, nº 1, pp. 73-82, 1995.

[4] J. B. Khurgin, and P. A. Morton, "Tunable wideband optical delay line based on balanced coupled resonator structures." *Optics letters*, vol. 34, num. 17, pp. 2655-2657, 2009.

[5] Y. Liu, et al., "Tuning Optimization of Ring Resonator Delays for Integrated Optical Beam Forming Networks," *Journal of Lightwave Technology*, vol. 35, no 22, p. 4954-4960, 2017.

[6] C. Xiang, et al., "Low-Loss Continuously Tunable Optical True Time Delay Based on Si3N4 Ring Resonators, " *IEEE Journal of Selected Topics in Quantum Electronics*, vol. 24, no 4, p. 1-9, 2018.

[7] D. Pérez, I. Gasulla, I. and J. Capmany, "Software-defined reconfigurable microwave photonics processor," *Optics Express*, vol. 23, pp. 14640-14654, 2015.

[8] J. Capmany, I Gasulla, and D. Pérez, "Microwave photonics: The programmable processor," *Nature Photonics*, vol. 10, pp. 6-8, 2016.

[9] L. Zhuang et al., "Programmable photonic signal processor chip for radiofrequency applications," *Optica*, vol. 2, pp. 854-859, 2015.

[10] D. Pérez, I. Gasulla, J. Capmany, and R. A. Soref, "Reconfigurable lattice mesh designs for programmable photonic processors," *Optics Express*, vol. 24, pp. 12093-12106, 2016.

[11] M. Reck, et al. Experimental realization of any discrete unitary operator. *Physical review letters*, 1994, vol. 73, no 1, p. 58, 1994.

[12] D. AB. Miller. Perfect optics with imperfect components. *Optica*, 2015, vol. 2, no 8, p. 747-750.

[13] W. R. Clements, et al., "Optimal design for universal multiport interferometers," *Optica*, 2016, vol. 3, no 12, p. 1460-1465.

[14] D. Pérez, et al., "Multipurpose silicon photonics signal processor core," *Nature Communications*, vol. 8, no. 636, 2017.

[15] D. Pérez, et al. Silicon photonics rectangular universal interferometer," *Laser & Photonics Reviews*, vol. 11, no. 6, 2017.

[16] D. Pérez, et al., "Towards programmable microwave photonics processors." *Journal of Lightwave Technology*, no. 99, 2778741, 2017.

[17] J. Carolan, et al., "Universal linear optics," Science vol. 349, no. 711, 2015

[18] D. Pérez, "Integrated microwave photonic processors using waveguide mesh cores", Ph.D. Thesis, 2017.

[19] M. Burla *et al.*, "On-chip, CMOS-compatible, hardware-compressive integrated photonic beamformer based on WDM," de Microwave Photonics (MWP), *2013 International Topical Meeting on, Alexandria*, VA, USA, 2013.

[20] M. Burla, et al., "Separate carrier tuning scheme for integrated optical delay lines in photonic beamformers," Microwave Photonics, 2011 International Topical Meeting on & Microwave Photonics Conference, Singapore , 2011.

[21] T.Horikawa *et al.*, "Low-loss silicon wire waveguides for optical integrated circuits," *Materials Research Society*, vol. 6, nª1, pp. 9-15, 2016.

[22] C. G. H. Roeloffzen *et al*., "Silicon nitride microwave photonic circuits," *Opt. Express*, vol. 21, pp. 22937-22961, 2013.

[23] Z. Sheng *et al.*, "A Compact and low-loss MMI coupler fabricated with CMOS Technology," *IEEE Photonics Journal*, vol. 4, nº6, pp. 22272-2277, 2012.

[24] G. W. Cong, *et al., "*Demonstration of a 3-dB directional coupler with enhanced robustness to gap variations for silicon wire waveguide." *Optics express*, vol. 22, nº 2, pp. 2051-2059, 2014.

[25] G. Micó, et al., "C-band linear propagation properties for a 300 nm film height silicon nitride photonics platform, " at *European Conference on integrated optics (ECIO 2017*), Eindhoven, the Netherlands, 2017.

[26] N. C. Harris, *et al*., "Efficient, compact and low loss thermo-optic phase shifter in silicon," *Optics Express*, vol. 22, nª9, pp. 10487-10493, 2014.

[27] Fang, *et al.*, "Ultralow power silicon photonics thermo-optic switch with suspended phase arms," *IEEE Photonics Technology Letters*, vol. 23, nº 8, 2011.

[28] C. W. Wong, *et al.,* "Strain-tunable silicon photonic band gap microcavities n optical waveguides," *Applied physics letters*, vol. 84, no. 8, pp. 1242-1244, 2004.

[29] M. W. Pruessner, *et al.,* "Effective index tuning in micro-opto-mechanical structures using gradient electric forces," in IEEE *Photonics society summer topical meeting series (SUM),* Newport Beach, CA, USA, 2016.

[30] H. Kogelnikm and R. V. Schmidt., Switched directional couplers with alternating Δβ," *IEEE Journal of Quantum Electronics*, 1976, vol. 12, no 7, p. 396-401.

[31] R.V. Schmidt and H. Kogelnik, "Electroptically switched coupler with stepped reversal using Ti diffused LiNbO3 waveguides," Appl. Phys. Lett., vol. 28, pp. 503-506, May 1976.

[32] R. C. Alferness and J.J. Veselka, "Simultaneous modulation and wavelength multiplexing with a tunable Ti: LiNbO3 directional coupler filter," *Electronics Letters*, 1985, vol. 21, no 11, p. 466-467.

[33] A. S. M. Supa'at, "Implementation of thermo-optic waveguide photonics switch using polymer material," at *Photonics (ICP), 2013 IEEE 4th International Conference on*. IEEE, 2013. p. 33-37.

[34] A. Sharkawy, et al. Electro-optical switching using coupled photonic crystal waveguides. *Optics Express*, vol. 10, no 20, p. 1048-1059, 2002.

[35] P. Orlandi, et al. Compact tunable directional couplers in SOI. at *CLEO: Science and Innovations*. Optical Society of America, 2013. p. JTu4A. 51., 2013

[36] K. Iizuka, *Engineering optics*. Springer Science & Business Media, 2013.

[37] G. Micó, et al., "Silicon nitride photonics: from visible to mid infrared wavelengths." at *SPIE Photonics West 2018 (Opto)* no.10537-9, 2018.

[38] H. Yamada, et al. Optical directional coupler based on Si-wire waveguides, in *Group IV Photonics, 2004. First IEEE International Conference on*. IEEE. p. 145-147, 2004.

[39] Z. Lu,, et al., Broadband silicon photonic directional coupler using asymmetric-waveguide based phase control. *Optics express*, vol. 23, no 3, p. 3795-3808, 2015.